

Research Article

Biosensitivity and Theoretical Electronic Structure Investigations on 3-(2-Hydroxyphenyl)-2-iminothiazolidin-4-one and Its Zn^{2+} and Cd^{2+} Metal Complexes

Zewdu Bezu Gemechu ¹, Boobalan Maria Susai ¹, Abi M. Taddesse,¹
Endale Teju Bedada ¹ and R. Ramamoorthy²

¹Department of Chemistry, College of Natural and Computational Sciences, Haramaya University, Dire Dawa, Ethiopia

²Department of Physics, St. Joseph's College (Autonomous), Tiruchirappalli, Tamil Nadu, India

Correspondence should be addressed to Zewdu Bezu Gemechu; zedo143@gmail.com

Received 14 September 2021; Accepted 1 October 2021; Published 31 October 2021

Academic Editor: Liviu Mitu

Copyright © 2021 Zewdu Bezu Gemechu et al. This is an open access article distributed under the Creative Commons Attribution License, which permits unrestricted use, distribution, and reproduction in any medium, provided the original work is properly cited.

A two-step cyclocondensation reaction has been carried out using 2-aminophenol with 2-chloroacetyl chloride to produce o-hydroxyphenyl chloroacetamide followed by treatment with KSCN in CH_3COCH_3 to produce the heterocyclic ligand 3-(2-hydroxyphenyl)-2-iminothiazolidin-4-one. The Zn^{2+} and Cd^{2+} complexes with a metal : ligands ratio of 1 : 4 were synthesized in ethanol using respective metal precursors with the title ligand. Antimicrobial activities of the ligand and its complexes were checked against some bacterial and fungal strains. The result evidenced better bioactive performance of the metal complex (though lower than the standard drug) than the free ligand against *Escherichia coli*, *Staphylococcus aureus*, and *Salmonella typhi* bacteria, as well as *Fusarium oxysporum* and *Aspergillus niger* fungal strains. Theoretical investigations on ligand and metal complexes help to infer the electronic structure behavior of them. Molecular geometry and bond order analysis provides detailed information on the nature of chemical structure and bonding. Molecular Electrostatic Potential (MEP) and atomic charge analysis claims evidence on charge distribution and electrophilic, nucleophilic reactive sites. Natural bond orbital analysis provides second-order perturbed stabilization interactions, orbital population, and their energies. Other theoretical properties such as hardness, softness, electron affinities, and ionization potential were derived and discussed in detail.

1. Introduction

In terms of structural and coordination compound chemistry, most metal complexes containing many heteroatoms in a membered ring receive a lot of attention. Because of their affluence of formation and flexibility, thiazolidinones have played an important role in the development of coordination chemistry, as they readily form stable complexes with most transition metals. Complexes make up a large number of biologically active compounds, and even the simplest forms of complexes have been used as model compounds in studies of bodily processes [1]. Imines are nitrogen carbon double bond compounds owing to their stability and structural similarity to natural biological

substances; imines are an essential class of compounds and are used as antipathogenic agents (bacteria, fungal) of which thiazolidinone are derivatives, which play an important role in medical science, and their unique physicochemical properties, which allow them to be used in a variety of other fields, put them ahead of other heterocyclic organics [2].

Furthermore, these compounds function as well-liked ligands, and their biosensitivity has been shown to increase with complexation. Thiazolidinones also serve as good ligands in the formation of metal complexes due to the presence of nitrogen, sulfur, and oxygen donors [3]. The strong antibacterial and antifungal properties of thiazolidinones sparked a lot of interest in the development of new compounds in this class. Ligands like

thiazolidinones and derivatives constrain certain bacterial and fungal strains to varying degrees [4–8].

Henceforth, the present work mainly focuses on the biological and computational probe of phenyl fused thiazolidinones based 3-(2-hydroxyphenyl)-2-iminothiazolidin-4-one ligand (L1) and its Zn^{2+} and Cd^{2+} (ZnL1 and CdL1) complexes, respectively. The experimental characterizations such as elemental, thermodynamical, and spectral (FTIR, UV-Vis, and NMR) attributes of the ligand and metal complexes had been reported in our earlier work [9]. In the present work, we are motivated to investigate the biological sensitivity and electronic structure characterization of those title systems in this work.

2. Materials and Methods

2.1. Synthesis of Ligand (L1) and Metal Complexes (ZnL1 and CdL1). The synthesis of 3-(2-hydroxyphenyl)-2-iminothiazolidin-4-one named L1 had been reported in our earlier work. The chemical structure of L1 was confirmed by various spectral characterizations. The L1 has been synthesized under double stage synthesis and its synthetic scheme is shown in Figure 1. The synthesis of Zn and Cd metal complexes of L1, namely, ZnL1 and CdL1, was reported in our prior work, where L1 was reported. The structure of ZnL1 and CdL1 was confirmed using elemental analysis, chloride test, UV-Vis, conductometric analysis, FTIR, and NMR spectral techniques [9].

2.2. Antimicrobial Sensitivity. The antibacterial sensitivity of the synthesized L1 and its ZnL1 and CdL1 complexes was tested in vitro using the paper disc diffusion method [10]. Antibacterial tests were performed on three important bacteria: *Escherichia coli* (Gram-negative), *Staphylococcus aureus* (Gram-positive), and *Salmonella typhi* (Gram-negative), as well as two fungi, *Fusarium oxysporum* and *Aspergillus niger*, which were tested using nutrient agar medium, with chloramphenicol and Bavistin standard antibiotic drugs serving as controls in antibactericidal and fungicidal studies, respectively. The diameter of the inhibition zones was measured, and the effectiveness of the synthesized compounds was assessed.

2.2.1. Preparation of Media and Sample Solution. *Escherichia coli*, *Staphylococcus aureus*, and *Salmonella typhi* bacteria were transferred from the culture and streaked for 24 hours at 37°C on Mueller-Hinton agar (MHA) plates. The bacteria were then transferred to autoclaved MHA that had been cooled to 45 degrees Celsius in a water bath and mixed vigorously by swirling the flasks. After that, the medium was poured into sterilized Petri dishes, solidified, and used. From stock cultures, mycelia plugs were transferred to PDA and incubated for 6 days. The fungi spores were then transferred to a 50 mL autoclaved PDA that had been cooled in a water bath to about 45°C. Finally, the spore suspension-containing media was poured into sterilized plates, solidified, and used for biotesting. The ligand and complex solutions were

prepared by dissolving their 10 mg samples in 1 ml DMSO, and 10 μ l and 20 μ l aliquots were used for biotest.

2.2.2. Antimicrobial Sensitivity Testing Procedure. The antibacterial sensitivity includes the following procedure: The Whatman no.1 filter paper was punctured with office puncture to obtain 6 mm diameter paper discs. The discs were sterilized in an oven at 180°C for 1 hour. Then, in two replications, 10 μ l and 20 μ l of compound solution were pipetted to the discs. The sample-impregnated paper discs were transferred with sterile forceps to a nutrient agar plate seeded with bacteria and incubated at 37°C for 24 hours. In antifungal sensitivity examination, similar procedures were followed excluding that paper discs impregnated with samples were transferred with sterile forceps to PDA seeded with spore suspensions of *Aspergillus niger* and *Rhizoctonia bataticola* at room temperature for 3 days [11].

2.3. Computation Profile. In general, the theoretical and computational investigations on molecular systems could help one to gain quantum chemical insight on the molecular electronic structure properties. The present work has been focused on computing, calculating, and inferring various electronic structure properties such as geometry, symmetry, energy, conformation, natural bonding (NBO), frontier molecular orbitals (FMO's), molecular electrostatics (MEP), charge, and additional associated molecular quantum chemical properties. The pure organic ligand L1 and its metal complex such as ZnL1 and CdL1 were examined using density functional theory (DFT). The conformational generation was performed using semiempirical level theory, namely, Austin Model 1 (AM1). For other electronic structure properties, L1 was treated with B3LYP/6-31+G(d) basis set. The metal complex was treated based on effective core potential (ECP) technique. In ZnL1 and CdL1 metal complex system, a dual basis set practice was incorporated simultaneously on both ligand and metal in a fashion like B3LYP/lanl2dz basis on Zn and Cd metal atoms, whereas for atoms of ligand B3LYP/6-31G(d) was applied. All the computations were performed using Gaussian 09W [12] theoretical code. The NBO enquiries were made by NBO 7.0 code [13].

3. Result and Discussion

3.1. Inferences from Antimicrobial Studies. Compounds L1, ZnL1, and CdL1 were screened for their antibacterial and antifungal activities in vitro following the procedure described elsewhere [10, 14] against *Escherichia coli* (Gram-negative), *Staphylococcus aureus* (Gram-positive), and *Salmonella typhi* (Gram-negative) bacteria and *Fusarium oxysporum* and *Aspergillus niger* fungi (1:1 v/v) using chloramphenicol (standard antibiotic drug) and Bavistin (standard antifungal drug) as references, respectively, and inhibition zone diameters of the respective compounds were measured as indicated in Table 1.

The antibacterial and antifungal activities of the synthesized complexes were lower than those of the reference

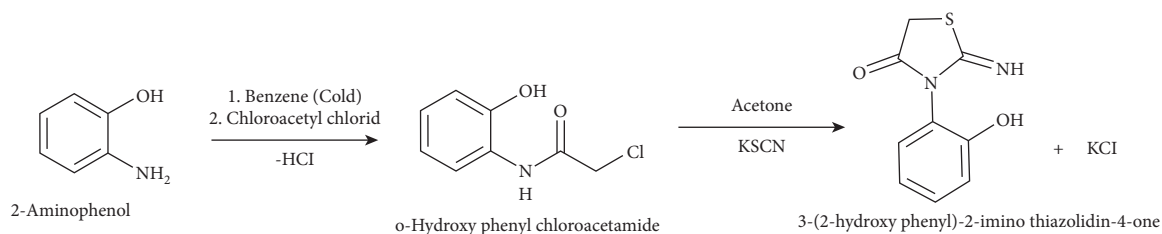


FIGURE 1: The synthetic scheme of L1.

TABLE 1: Bacterial and fungal growth inhibition zone (mm).

Compounds	Inhibition zone (mm)									
	<i>Escherichia coli</i>		<i>Staphylococcus aureus</i>		<i>Salmonella typhi</i>		<i>Fusarium oxysporum</i>		<i>Aspergillus niger</i>	
	10 μ L	20 μ L	10 μ L	20 μ L	10 μ L	20 μ L	10 μ L	20 μ L	10 μ L	20 μ L
L1	10	12	13	14	15	17	11	14	13	14
ZnL1	11	14	16	17	19	10	14	16	14	16
CdL1	10	13	17	19	21	22	11	12	10	11
Chloramphenicol	24	27	23	24	23	25	—	—	—	—
Bavistin	—	—	—	—	—	—	25	25	27	28
DMSO	—	—	—	—	—	—	—	—	—	—

Note: the values of inhibition zones are average of triplications.

drugs. Compounds L1, ZnL1, and CdL1 are active against all microbes tested. As a result, higher sensitivity has been observed in complexes than in free ligands, owing to chelation theory [1, 10]. The synthesized complexes inhibited all of the pathogens. The polarities of the metal ions are reduced during coordination due to ligand orbital overlap and partial sharing of the positive charge of the metal ions with the ligand donor atoms. This may increase the lipophilic nature of the metal complexes, allowing them to permeate the lipid membrane and thus be active in some bacteria and fungi while causing minor inhibition in the ligand. While chelation is not the only criterion for antimicrobial sensitivity, it may be a complex combination of several factors, including the nature of the metal ion and the ligand, the geometry of the metal complex, lipophilicity, and steric and pharmacokinetic factors. However, one must be cautious to examine the degree of toxicity of these metal complexes against biological array to proceed further since metal complexes have heavy metals.

3.2. Dry Lab Investigations

3.2.1. Conformational Analysis. The conformational analysis helps the system to identify the ground state conformer. The presence of rotatable single bond, bond angle, and dihedral bond could result in producing various conformers with different structural orientation with corresponding energy. In the present L1 system, a rigorous 3D conformational search has been executed under AM1 semiempirical level theory [15, 16]. In a 3D scan, one dimension represents energy coordinate and the other two orientations represent two dihedral scan coordinates. The pictorial projection is given in Figure 2. Scan coordinate-1 (SC-1) was taken from

$C_{13}-N_{18}-C_4-C_3$ and the SC-2 was taken from $H_{12}-O_{11}-C_5-C_6$ dihedral coordinate due to the presence of single bond connectivity which obviously could produce large number of conformers from set of rotational instructions. The connecting junction of five and six membered rings, namely, $N_{18}-C_4$, and another bonding coordinate $O_{11}-C_5$ would be static on the scan coordinate. However, other moieties connected with either side of the terminal of these said bonds in the dihedral will rotate 360 degrees by 10 degrees of increment up to 36 steps. This rotational instruction would produce 1369 conformers with various energy levels as shown in Figure 2. The change in the energy level is shown in the color graph ranging from red (high energy) to purple (low energy). The high energy conformer has been identified in one location when $SC-1 = 28.9553/SC-2 = 22.0012$ in 3D scan map as mentioned at the apex position in the 3D color graph. The energy of this conformer was found to be 0.015627 hartree. Stereochemically as expected, it shows planner structure and the figure has been shown here. The steric and noncovalent van der Waals interaction could be responsible for this energy hike when five and six membered rings are in planar geometry. The ground state minimum energy conformers were marked and shown in the figure. Large numbers of stable conformers were observed in this scan coordinate out of 1369 conformers in which all of them exhibit the same structural orientation. As expected, the five and six membered rings were perpendicular to each other and eventually had less steric and noncovalent van der Waals interaction which results in minimization of energy. The energy of stable conformer was found to be -0.014669 hartree and its projection is shown in the figure. The SC-1 and SC-2 orientations of ground state conformer appeared at -71.0446 and -177.9987 degrees, respectively. The relative energy was found to be 0.030296 hartree.

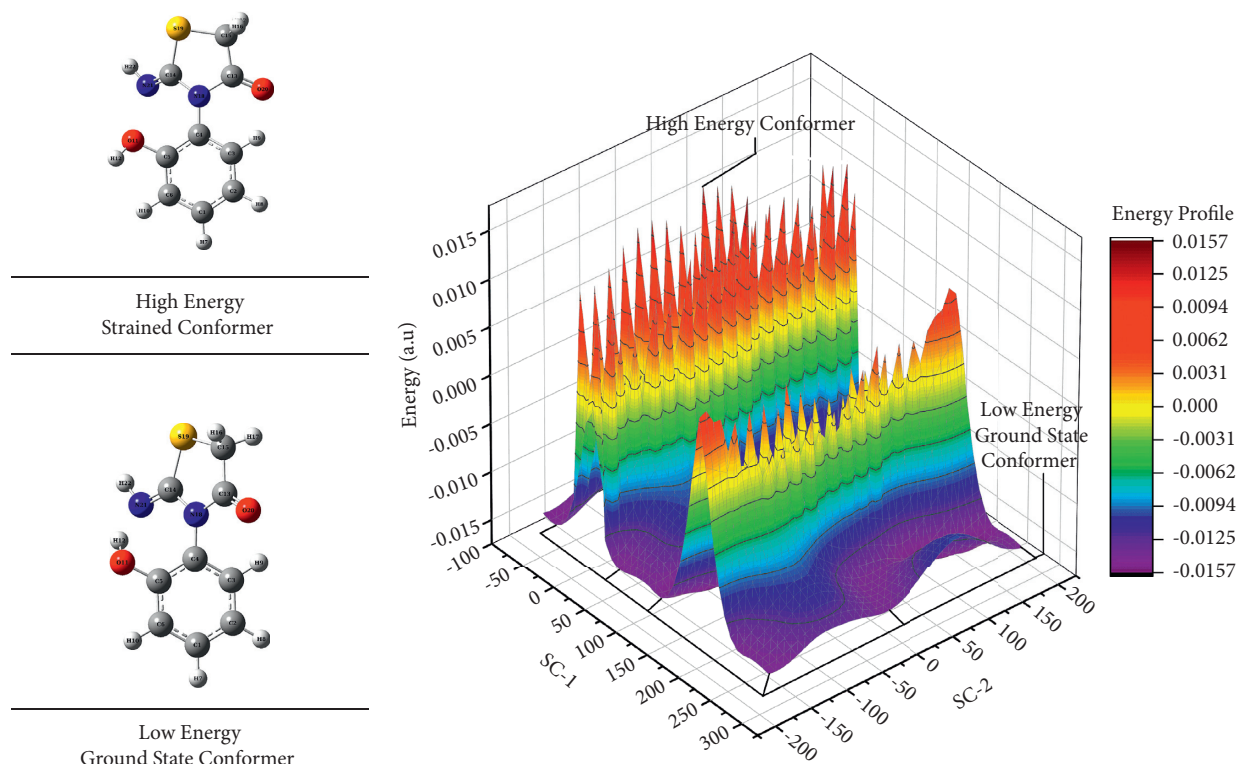


FIGURE 2: 3D scan coordinates on SC1 and SC2 with respect to energy using AM1 level.

3.2.2. Optimized Geometry. The ground state electronic structure properties of the title molecules were extracted from optimized ground state molecular geometry. Optimized geometrical parameters include spatial vectors such as bond length, bond angle, and dihedral angle of a given system. The geometrical parameters of L1 are given in Table 2. The parameters of ZnL1 and CdL1 are given in Supplementary Material S1. The projections of their geometry are shown in Figures 3–5, respectively. The six membered benzenoid aromatic system with conjugation and the five membered heterocyclic system which has nonaromatic character are reflected in their bond order and bond length. Any aromatic system could have C-C bond length ranging from 1.390 to 1.410 Å. In benzene, it is found to be 1.39 Å exactly. In L1, the fused benzene moiety has 1.399 to 1.401 Å of aromatic C-C length. The trend between bond length and bond order could be reciprocally related. The same has been observed here. The aromatic C-C bond includes both end-end and side-side overlap of valence “p” orbital of carbon which resulted in formation of “ σ ” and “ π ” of bonds, respectively. These two types of overlap eventually reduce the bond length and increase the bond order with increased bond dissociation energy in comparison to non-aromatic C-C bond which has pure “ σ ” bond character. This trend has been observed in five membered heterocyclic moiety of L1 which has C13-C15 “ σ ” bond nature with 1.524 Å bond length and 0.995 and 1.023 fuzzy and Laplacian bond orders, respectively [17].

The ECP technique has been implemented to optimize the metal complex. This metal complex numerical optimization was tedious; henceforth we used T_d constrained,

symmetry-off, very tight Berny algorithm to get the ground state stationary point. The ground state was verified by existence of positive frequencies at potential energy surface. In accordance with the experimental evidences, all the four ligands were coordinated with the metal (Zn, Cd) under T_d symmetry. In ZnL1 system, the central Zn atom has tetrahedral arrangement and all the four lobes are connected with four different oxygen atoms of four hydroxyl groups of phenyl moiety, respectively. The bond length of Zn1-O2 and Zn1-O23 was found to be 1.991 Å, whereas that of Zn1-O44 and Zn1-O65 was observed as 1.989 Å. The fuzzy bond order was found to be 1.013 and 1.026 (fuzzy) and Laplacian values were observed as 0.217 and 0.219, respectively. These theoretical values help us to understand the strength of the metal-ligand bonds and their nature. Similarly, in CdL1, the Cd has T_d arrangement surrounded by four ligands. The bond length among Cd1-O2, Cd1-O23, Cd1-O44, and Cd1-O65 was found to be 2.191, 2.188, 2.191, and 2.192 Å, respectively. The calculated fuzzy bond order was observed as 1.036, 1.034, 1.093, and 1.103 respectively. The Laplacian scale bond order was found to be 0.207, 0.209, 0.209, and 0.221 respectively. Hence, these results conclude that the strength of both Zn-O and Cd-O could be equally comparable except bond length.

3.2.3. Fragmented FMO Analysis. Frontier molecular orbital analysis is a traditional technique to understand how electrons could be interacting between bonding and antibonding molecular orbitals. Chemical and electronic properties such as hardness, softness, reactivity, and

TABLE 2: Optimized geometrical parameters and bond order of L1.

Bond length (Å)	Fuzzy	Laplacian	Bond angle (°)		Dihedral angle (°)		
C1-C2	1.399	1.444	1.538	C1-C6-C5	120.81	C5-C4-N18-C14	-56.72
C1-C6	1.392	1.481	1.566	C5-O11-H12	107.28	C4-C5-C6-C1	-0.85
C2-C3	1.392	1.472	1.557	C15-C13-N18	112.16	O11-C5-C6-C1	-179.69
C3-C4	1.400	1.366	1.505	C15-C13-O20	122.65	N18-C13-C15-S19	0.15
C4-C5	1.409	1.303	1.494	N18-C13-O20	125.19	O20-C13-C15-S19	179.60
C4-N18	1.446	1.063	0.688	N18-C14-S19	111.59	C15-C13-N18-C4	175.17
C5-C6	1.401	1.352	1.549	N18-C14-N21	121.83	C15-C13-N18-C14	-2.87
C5-O11	1.362	1.350	0.535	S19-C14-N21	126.56	O20-C13-N18-C4	-4.27
O11-H12	0.987	0.712	0.432	C13-C15-S19	107.62	O20-C13-N18-C14	177.69
C13-C15	1.524	0.995	1.023	C4-N18-C13	120.42	S19-C14-N18-C4	-173.67
C13-N18	1.401	1.194	0.924	C4-N18-C14	123.21	S19-C14-N18-C13	4.31
C13-O20	1.212	2.003	1.216	C13-N18-C14	116.34	N21-C14-N18-C4	7.94
C14-N18	1.398	1.171	0.940	C14-S19-C15	92.14	N21-C14-N18-C13	-174.08
C14-S19	1.787	1.176	0.825	C14-N21-H22	112.83	N18-C14-S19-C15	-3.44
C14-N21	1.278	1.828	1.646	Dihedral angle (°)		N21-C14-S19-C15	174.85
C15-S19	1.826	1.176	0.633	C6-C1-C2-C3	1.36	N18-C14-N21-H22	-179.83
N21-H22	1.019	0.852	0.698	C2-C1-C6-C5	-1.00	S19-C14-N21-H22	2.03
Bond angle (°)			C1-C2-C3-C4	0.14	C13-C15-S19-C14	1.82	
C2-C1-C6	120.20		C2-C3-C4-C5	-2.01			
C1-C2-C3	119.51		C2-C3-C4-N18	175.10			
C2-C3-C4	120.57		C3-C4-C5-C6	2.34			
C3-C4-C5	120.05		C3-C4-C5-O11	-178.88			
C3-C4-N18	118.16		N18-C4-C5-C6	-174.65			
C5-C4-N18	121.73		N18-C4-C5-O11	4.13			
C4-C5-C6	118.82		C3-C4-N18-C13	-51.67			
C4-C5-O11	122.94		C3-C4-N18-C14	126.23			
C6-C5-O11	118.24		C5-C4-N18-C13	125.38			

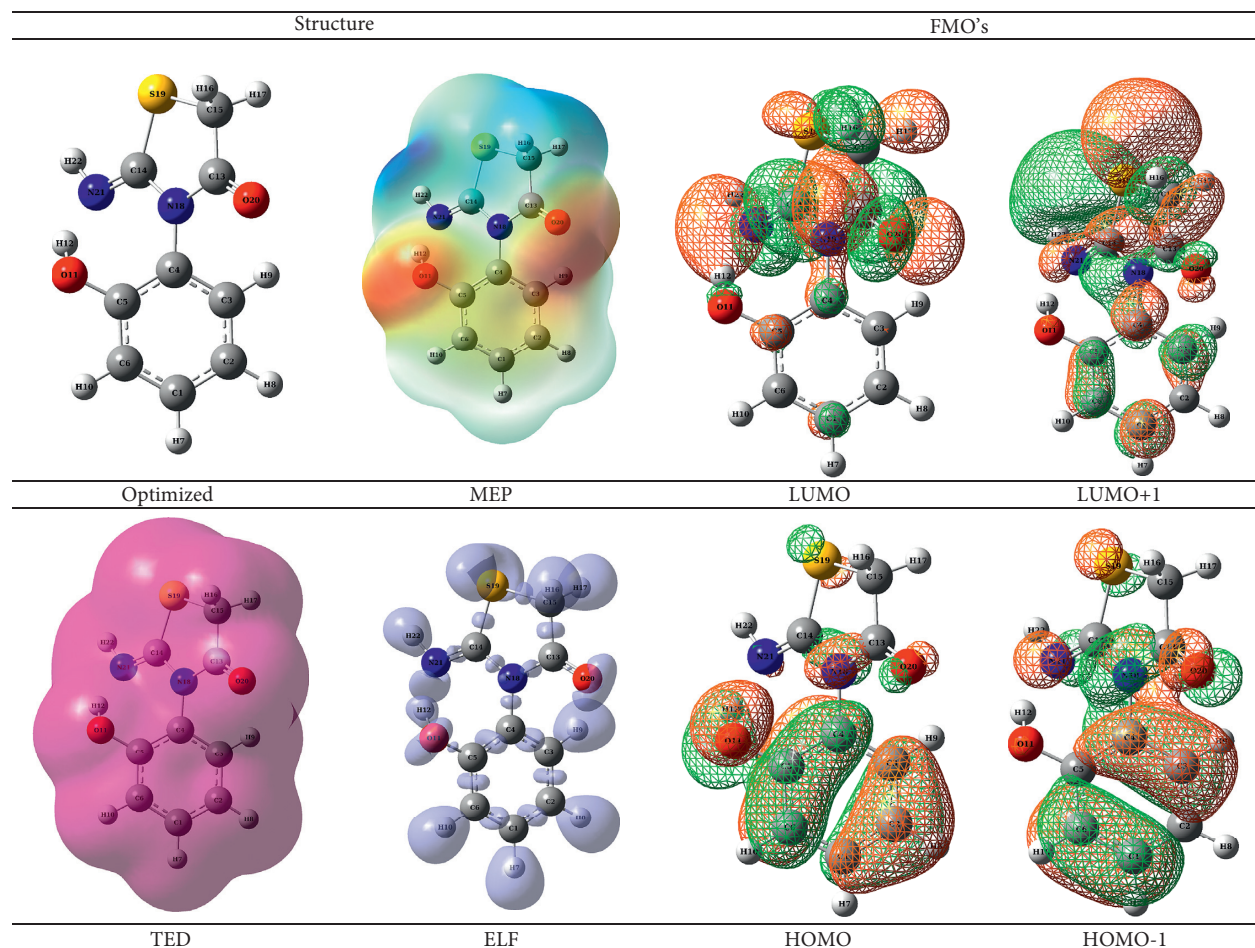


FIGURE 3: Optimized structure, FMOs, surfaces, and ELF plots of L1.

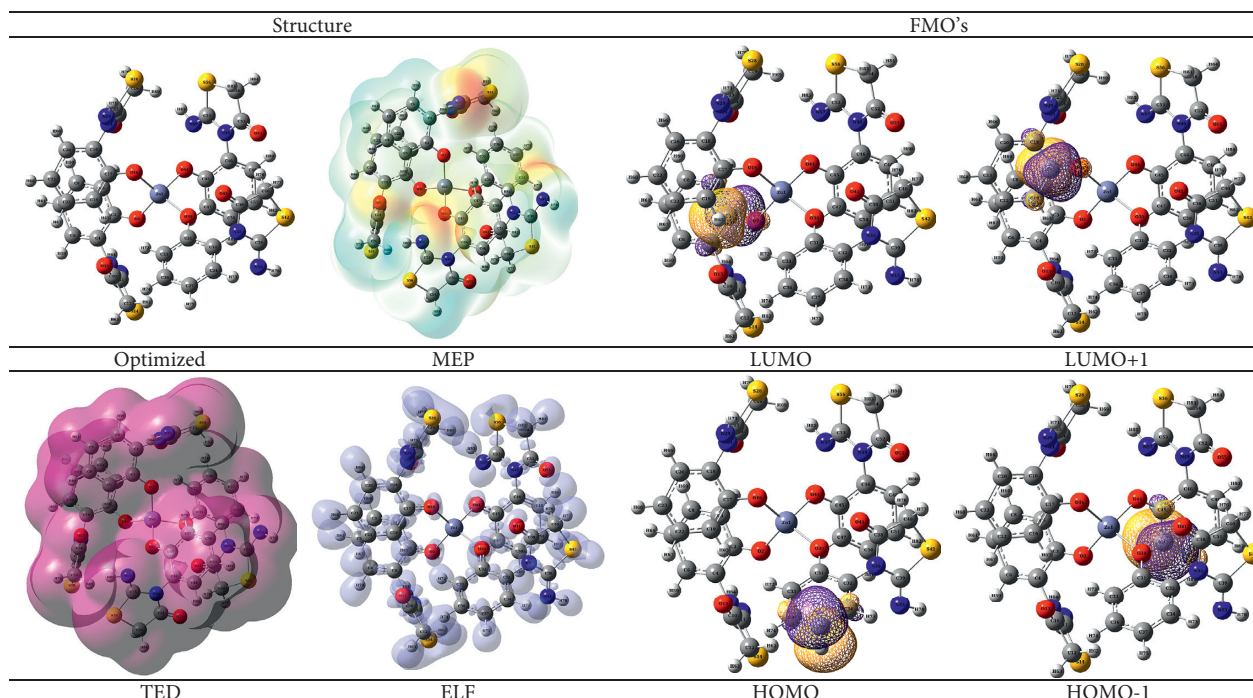


FIGURE 4: Optimized structure, FMOs, surfaces, and ELF plots of ZnL1.

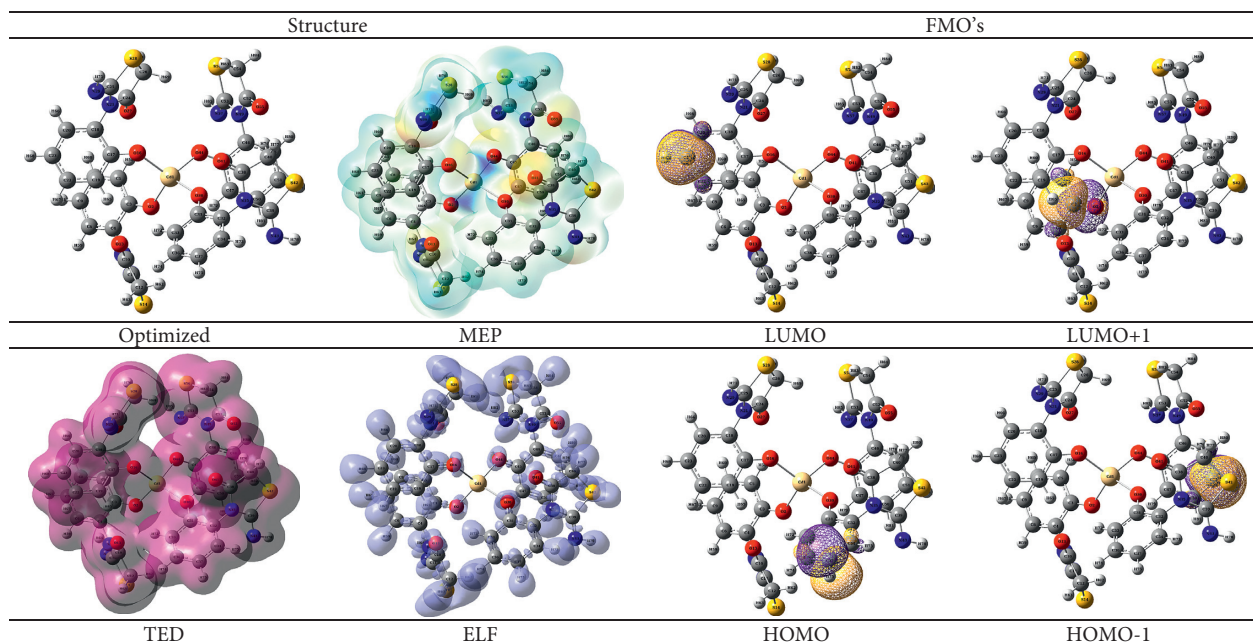


FIGURE 5: Optimized structure, FMOs, surfaces, and ELF plots of CdL1.

charge transport depend on the FMO gap. The FMO gap values among HOMO-1, HOMO, LUMO, and LUMO+1 are tabulated in Table 3 and the surface projections are given in Figures 3–5. The atomic contributions to FMOs are listed Table 4. ΔE_{L-H} of L1 was found to be 5.06 eV. In ZnL1 and CdL1, these values were 0.5023 eV and 0.4624 eV, respectively. A more significant dropping has been observed in metal complex compared to pure L1. The

atomic contribution on FMO formation for L1 largely comes from atom “C” with 80% on HOMO and 52% on LUMO. Atom “O and N” contributes second and third, respectively. In the case of ZnL1 and CdL1, the HOMO and LUMO were highly contributed by “C” as in L1. But more contributions were observed by “O” in ZnL1 and CdL1 compared to pure L1. Central metals “Zn and Cd” have 0% and 1% contribution in HOMO and LUMO

formation. The “H” atom has no contribution in all the three systems. The position of lobes in L1 at HOMO was localized around six membered ring and LUMO was around five membered ring. Since the lobes of the orbitals are perpendicular to plane of the molecular symmetry, they must be $\pi \rightarrow \pi^*$ transition [18–20]. The same type of transition is observed in ZnL1 and CdL1 transitions.

3.2.4. MEP and Atomic Charge Analysis. The MEP and atomic charge analysis has been carried out for L1, ZnL1, and CdL1. The MEP surface of L1 is shown in Figure 3 and the computed atomic charges are listed in Table 5. The MEP of ZnL1 and CdL1 is shown in Figures 4 and 5, respectively. The calculated charges are listed in Supplementary Material 2. Various atomic charge schemes such as Mulliken, atomic tensor polar (ATP), Hirshfeld, and natural population analysis (NPA) were computed for all the three systems. The mathematical formulation of MEP and various atomic changes is as follows:

$$V(r) = \frac{Z_A}{|R_A - r|} - \int \frac{\rho(r')}{|r' - r|^3} r' \quad (1)$$

The notations in the equation can be given as follows: Z_A represents the charge of the nucleus “A” located at R_A , $\rho(r')$ specifies the electronic density of the system, and r' represents the trivial integral variable. Generally, the MEP color surface ranging from red to blue indicates the more electron populated region (electrophilic site) to lesser electron population region (nucleophilic site). In L1, the electro-positive region was observed at five membered ring and electronegative region was observed in six membered ring. Around O11 and O20, the surface is rich in red and at N18, N21, and S19 it became blue. This trend is reflected in point charge analysis as well and discussed hereunder. Similarly, in ZnL1 and Cd L1, the position around oxygen atoms exhibits red surface and nitrogen and sulfur region shows blue. This imprint could help one to understand the nature reactive in these systems when introduced to a Lewis acid and base. The total electron density map (TED) could project the size occupied as a whole system in space; eventually molecular electron density volume related attributes could be derived.

Furthermore, the theoretical foundation of Mulliken point charge could be given as

$$q_A = Z_A - \sum_i n_{i,A} = Z_A - \sum_i \eta_i \sum_{a \in A} \Theta_{i,a} \quad (2)$$

where η denotes orbital occupation number and $n_{i,A}$ states the contribution from orbital “i.” It is highly basis set dependent.

The ATP model could be provided as follows:

$$q_i = \frac{1}{3} \left(\frac{\partial \mu_x}{\partial x_i} + \frac{\partial \mu_y}{\partial y_i} + \frac{\partial \mu_z}{\partial z_i} \right), \quad (3)$$

where “ μ ” is the dipole moment of the given system and x_i , y_i , and z_i denote vectors of “ i^{th} ” atom.

Hirshfeld would be represented by

$$q_A = - \int w_A^{\text{Hirsh}}(r) \rho_{\text{def}}(r) dr. \quad (4)$$

For NPA, it can be given as follows:

$$q_A^{(N)} = \sum_i q_i^{(N)}, \quad (5)$$

where $q_A^{(N)}$ denotes natural electron population on overlap free natural atomic orbital [21–24].

Though the Mulliken population analysis is a traditional method to calculate point charges, it is highly basis set dependent. Since the L1 was an organic system which was treated with B3LYP/6-31+G(d), a promising level basis set, the results were comparable with other methods except in atoms such as C3, C5, C14, and S19 where a negative reciprocal charge magnitude has been observed. However, the rest of the atoms are in good agreement with other point charge theories. In accordance with electronegativity, the excess electron population is expected in heteroatoms such as O11, N18, S19, O20, and N21. The same was observed in all the atomic charge theories with significant increased electron population as mentioned in Table 5.

In ZnL1 and CdL1 complexes, the L1 is arranged in a T_d arrangement with 1:4 metal cum ligand stoichiometry. The Zn and Cd metal atoms nearly have more than a unity positive charge except Hirshfeld method. In ZnL1, more electron population has been observed in all heteroatoms of four ligands. But, in CdL1, less electron population trend has been observed in heteroatoms in all the theories except in few atoms in comparison with ZnL1. Electron localization function (ELF) is a method to calibrate electron at the neighboring space with reference to electron localized at a given point with the same spin. The ELF values in pi delocalized region fall around less than 0.65 and in sigma bond region they were noticed to be greater than 0.70 to 0.99.

3.2.5. NBO Analysis. The natural bond orbital analysis method is an efficient technique to gain detailed chemical insight on chemical bonding, point charges, and second-order perturbed stabilization interactions. The stabilization interaction chemistry between Lewis donor orbitals and non-Lewis acceptor orbitals could help one to understand how a molecule could attain stabilized electronic stationary point structurally. The present study provides detailed NBO information on both ligand L1 and its metal complexes, namely, ZnL1 and CdL1, respectively. The figure incorporated first five strong stabilization interactions of L1, ZnL1, and CdL1, shown in Tables 6–8, respectively.

The mathematical background of NBO interaction could be given as follows:

$$\Delta E_{ij}^{(2)} = - \frac{q_i |F_{ij}|^2}{\epsilon_j^{(NL)} - \epsilon_i^{(L)}}, \quad (6)$$

where $\Delta E_{ij}^{(2)}$ denotes stabilization energy of the corresponding contacts, q_i specifies the population of the Lewis orbital, and F_{ij} denotes Fock matrix which comes from the

TABLE 3: Other electronic structure properties of L1, ZnL1, and CdL1.

Properties	L1	ZnL1	CdL1
Energy	-1005.944951 hartree	-4086.75259 hartree	-4069.258684 hartree
Dipole moment	3.2612 Debye	3.7202 Debye	2.8688 Debye
Polarizability	144.2924 au	508.9803 au	584.1757 au
Hyperpolarizability	341.6341 au	5058.6180 au	3966.6924 au
LUMO+1	-1.0270 eV	-0.8602 eV	-0.8302 eV
LUMO	-1.3755 eV	-4.8039 eV	-4.8239 eV
HOMO	-6.4355 eV	-5.3063 eV	-5.2863 eV
HOMO-1	-7.0029 eV	-5.5721 eV	-5.5221 eV
ΔE_{L-H}	5.0599 eV	0.5023 eV	0.4624 eV
Ionization potential (IP)	6.4355 eV	5.3063 eV	5.2863 eV
Electron affinity (A)	1.3755 eV	4.8039 eV	4.8201 eV
Global hardness (η)	2.5300	0.2512	0.2331
Global softness (ν)	0.1976	3.9808	4.2900
Electronegativity (χ)	3.9055	5.0551	4.7881
Chemical potential (μ)	-3.9055	-5.0551	-4.7881
Global electrophilicity (ω)	3.0144	50.8639	49.1761

TABLE 4: Percentage fragmentation contributions in FMO.

Atoms/FMO	FMO of L1 systems					
	C	N	O	S	H	
L+1	24	5	0	71	5	
L	52	20	18	5	5	
H	80	1	19	0	0	
H-1	85	10	4	1	0	
Atoms/FMO	FMO of ZnL1 systems					
	C	N	O	S	H	Zn
L+1	90	1	4	2	1	1
L	75	1	24	0	0	0
H	75	1	24	0	0	0
H-1	75	1	22	0	0	1
Atoms/FMO	FMO of CdL1 systems					
	C	N	O	S	H	Cd
L+1	81	3	8	4	3	0
L	72	1	26	0	0	1
H	73	1	24	0	0	1
H-1	74	2	24	0	0	1

result of Lewis and non-Lewis mixing in delocalization. $\varepsilon_i^{(L)}$, $\varepsilon_j^{(NL)}$ describe the orbital energy of donor and acceptor fragments. The stabilization energy is directly accompanied with the energy gap of Lewis and non-Lewis moieties projection [25–27].

In L1 system, highest five stabilizations were observed due to lone pair (LP) $\rightarrow \pi^*$ interactions. The LP was contributed from O11, N18, O20, and S19 atomic Lewis moieties. The first interaction was stabilized by 35.62 kJ/mole, where the donor has 1.86916e population 0.34 au energy difference. Since the donation comes from LP, the % ED partition is zero; but, in acceptor, C5 has more electron density distribution than C4. The natural localized molecular orbital dipole (NLMO) was found to be 1.18 Debye on the Lewis. The second stabilization energy was observed by 34.32 kJ/mole and the difference with the first one was found to be 1.3 kJ/mole. Large stabilization energy differences were observed between second and third interactions (2.33 kJ/mole) and between fourth and fifth interactions (5.17 kJ/mole), respectively.

Similarly, in ZnL1, the following Lewis donor was observed such as C5, C47, and C37 atoms. The apex stabilization was attained by LP(C5) $\rightarrow \pi^*(O2-C3)$ interaction. The electron density partition in non-Lewis acceptor was found to be 78.06% in C3 and 21.94% in O2. The stabilization energy difference between first and second interactions was found to be 21.6 kJ/mole. Likewise, the stabilization difference between the second and third interactions was found to be 78.47 kJ/mole. However, differences between third and fourth interactions and between fourth and fifth interactions were significantly less. The first and third Lewis donors are identical to each other, yet their corresponding non-Lewis acceptors are different. The same is true in the case of second and fourth Lewis donors.

In the case of CdL1, the donor Lewis moieties were found to be C9, C37, and C51 with more than 0.9e population. The highest stabilization interaction was found to be 104.04 kJ/mole, which is very less in comparison with ZnL1. The second stabilization energy was found to be 96.58 due to LP(1) C37 $\rightarrow \pi^*(C32-C34)$. Around 7.46 kJ/mole stabilization

TABLE 5: Various theoretical atomic charges on L1.

Atom	Mulliken	APT	Hirshfeld	NPA
C1	-0.1575	0.0588	-0.0349	-0.2161
C2	-0.3308	-0.1279	-0.0509	-0.2676
C3	0.2299	0.0248	-0.0414	-0.2060
C4	0.1652	0.1766	0.0218	0.0700
C5	-0.3925	0.4659	0.0724	0.3322
C6	-0.0108	-0.1133	-0.0514	-0.2754
H7	0.1823	0.0285	0.0482	0.2474
H8	0.1822	0.0276	0.0461	0.2471
H9	0.1915	0.0463	0.0472	0.2496
H10	0.1983	0.0469	0.0516	0.2583
O11	-0.6771	-0.7401	-0.2281	-0.6878
H12	0.5166	0.3966	0.1195	0.5068
C13	0.5192	1.0280	0.1943	0.6962
C14	-0.1232	1.0403	0.1372	0.2708
C15	-0.8349	0.0239	-0.0266	-0.6971
H16	0.2826	0.0301	0.0637	0.2940
H17	0.2787	0.0239	0.0621	0.2949
N18	0.0675	-0.8775	-0.0422	-0.5345
S19	0.4487	-0.2268	-0.0074	-0.2792
O20	-0.4159	-0.7463	-0.2682	-0.5524
N21	-0.6904	-0.7737	-0.2289	-0.6999
H22	0.3705	0.1874	0.1160	0.3902

TABLE 6: NBO profile of L1.

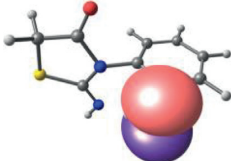

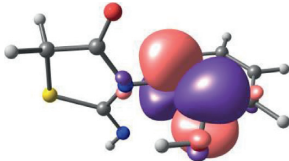
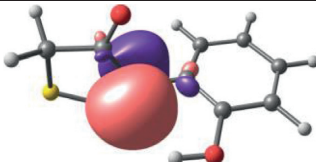
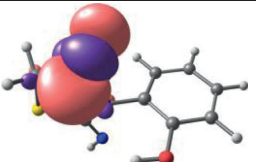
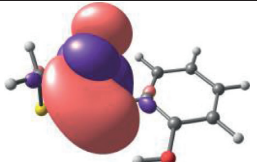
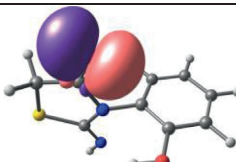
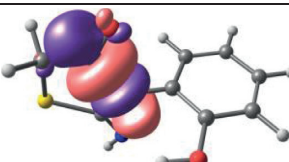
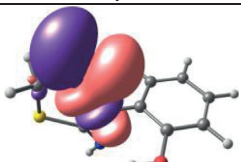
S. no.	Donor	Acceptor	Stabilization
01	 <p>LP (2) O11/E_D (i): 1.86916e OE ($\epsilon_i^{(L)}$): -0.32938 a.u $\%E_D$ P: -/NLMOD: 1.18D</p>	 <p>π^*C4- C5/E_D (j): 0.40876e OE ($\epsilon_j^{(NL)}$): 0.01441 a.u $\%E_D$ P: 43.15$_{C4}$-56.85$_{C5}$</p>	 <p>$E(2)$ kJ mol$^{-1}$: 35.62 $E(j)-E(i)$: 0.34 a.u $F(i,j)$: 0.099 a.u</p>
02	 <p>LP (1) N 18/E_D (i): 1.68286e OE ($\epsilon_i^{(L)}$): -0.31154 a.u $\%E_D$ P: -/NLMOD: 1.63D</p>	 <p>π^*C13- O 20/E_D (j): 0.20748e OE ($\epsilon_j^{(NL)}$): 0.01337 a.u $\%E_D$ P: 68.17$_{C13}$-31.83$_{O20}$</p>	 <p>$E(2)$ kJ mol$^{-1}$: 34.32 $E(j)-E(i)$: 0.32 a.u $F(i,j)$: 0.094 a.u</p>
03	 <p>LP (2) O 20/E_D (i): 1.84296e OE ($\epsilon_i^{(L)}$): -0.28193 a.u $\%E_D$ P: -/NLMOD: 1.31D</p>	 <p>σ^*C13- N 18/E_D (j): 0.10575e OE ($\epsilon_j^{(NL)}$): 0.32151 a.u $\%E_D$ P: 63.64$_{C13}$-36.36$_{N18}$</p>	 <p>$E(2)$ kJ mol$^{-1}$: 31.99 $E(j)-E(i)$: 0.60 a.u $F(i,j)$: 0.124 a.u</p>

TABLE 6: Continued.


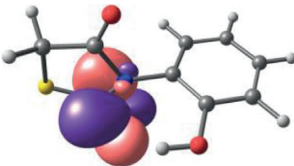
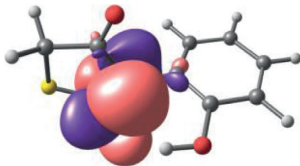
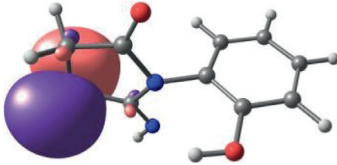
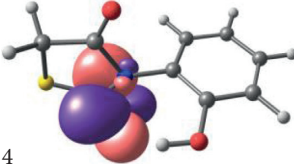
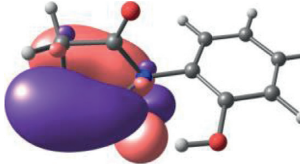
S. no.	Donor	Acceptor	Stabilization
04	 <p>LP (1) N 18/E_D (i): 1.68286e OE ($\epsilon_i^{(L)}$): -0.31154 a.u %E_D P: -/NLMOD: 1.63D</p>	 <p>π^*C14- N 21/E_D (j): 0.24930e OE ($\epsilon_j^{(NL)}$): -0.01791 a.u %E_D P: 60.08$_{C14}$-39.92$_{N21}$</p>	 <p>$E(2)$ kJ mol$^{-1}$: 31.35 $E(j)-E(i)$: 0.29 a.u $F(i,j)$: 0.086 a.u</p>
05	 <p>LP (2) S 19/E_D (i): 1.84334e OE ($\epsilon_i^{(L)}$): -0.27665 a.u %E_D P: -/NLMOD: 1.33D</p>	 <p>4 π^*C14- N 21/E_D (j): 0.24930e OE ($\epsilon_j^{(NL)}$): -0.01791 a.u %E_D P: 60.08$_{C14}$-39.92$_{N21}$</p>	 <p>$E(2)$ kJ mol$^{-1}$: 26.18 $E(j)-E(i)$: 0.26 a.u $F(i,j)$: 0.073 a.u</p>

TABLE 7: NBO profile of ZnL1.

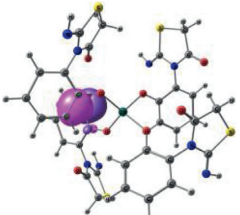
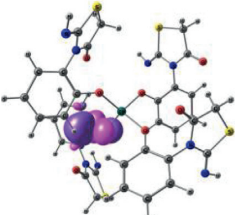
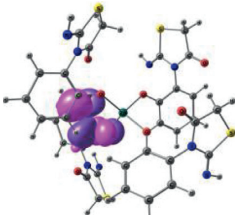
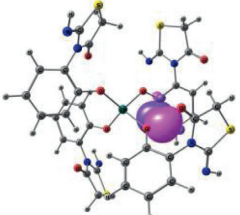
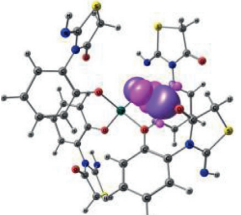
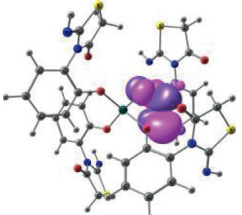
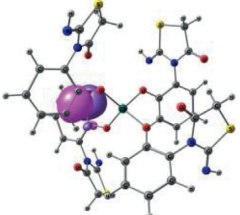
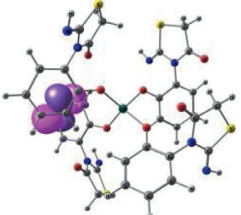
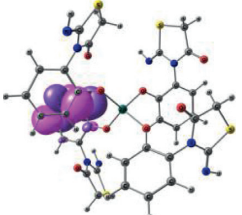
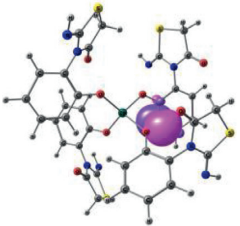
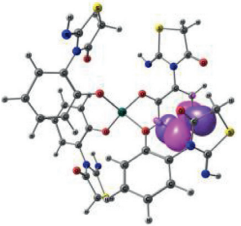
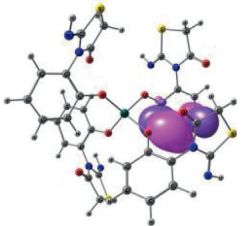
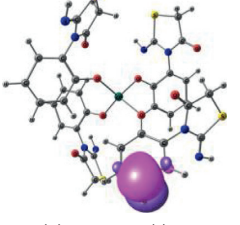
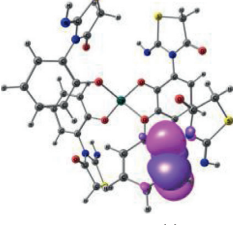
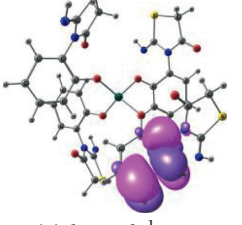
S. no.	Donor	Acceptor	Stabilization
01	 <p>LP (1) C5/E_D (i): 0.9890e OE ($\epsilon_i^{(L)}$): -0.1148 a.u %E_D P: -/NLMOD: 0.00D</p>	 <p>π^*O2-C3/E_D (j): 0.5776e OE ($\epsilon_j^{(NL)}$): -0.0255 a.u %E_D P: 21.94$_{O2}$-78.06$_{C3}$</p>	 <p>$E(2)$ kJ mol$^{-1}$: 201.42 $E(j)-E(i)$: 0.09 a.u $F(i,j)$: 0.120 a.u</p>
02	 <p>LP(1) C47/E_D (i): 0.9916e OE ($\epsilon_i^{(L)}$): -0.1142 a.u %E_D P: -/NLMOD: 0.00D</p>	 <p>π^*O44-C45/E_D (j): 0.5326e OE ($\epsilon_j^{(NL)}$): -0.0184 a.u %E_D P: 23.27$_{O44}$-76.73$_{C45}$</p>	 <p>$E(2)$ kJ mol$^{-1}$: 179.82 $E(j)-E(i)$: 0.10 a.u $F(i,j)$: 0.117 a.u</p>
03	 <p>LP (1) C5/E_D (i): 0.9890e OE ($\epsilon_i^{(L)}$): -0.1148 a.u %E_D P: -/NLMOD: 0.00D</p>	 <p>π^*C8-C9/E_D (j): 0.26324e OE ($\epsilon_j^{(NL)}$): 0.0243 a.u %E_D P: 50.87$_{C8}$-49.13$_{C9}$</p>	 <p>$E(2)$ kJ mol$^{-1}$: 101.35 $E(j)-E(i)$: 0.14 a.u $F(i,j)$: 0.106 a.u</p>

TABLE 7: Continued.

S. no.	Donor	Acceptor	Stabilization
04	 <p>LP(1) C47/E_D (i): 0.9916e OE ($\epsilon_i^{(L)}$): -0.1142 a.u %E_D P: -/NLMOD: 0.00D</p>	 <p>π^*C50-C51/E_D (j): 0.2728e OE ($\epsilon_j^{(NL)}$): 0.0245a.u %E_D P: 49.84$_{C50}$-50.16$_{C51}$</p>	 <p>E(2) kJ mol⁻¹:101.10 E(j)-E(i): 0.14 a.u F(i,j): 0.106 a.u</p>
05	 <p>LP(1)C37/E_D (i): 0.9858e OE ($\epsilon_i^{(L)}$): -0.1090a.u %E_D P: -/NLMOD: 19.44D</p>	 <p>π^*C32-C34/E_D (j): 0.3123e OE ($\epsilon_j^{(NL)}$): 0.0378 a.u %E_D P: 46.79$_{C32}$-53.21$_{C34}$</p>	 <p>E(2) kJ mol⁻¹: 96.16 E(j)-E(i): 0.15 a.u F(i,j): 0.106 a.u</p>

energy difference was observed in first and second donor acceptor interaction. However, there was no significant difference observed between second and third interactions and between fourth and fifth interactions. The first and fifth Lewis donor moieties and third and fourth donor moieties have similar second-order perturbation properties. But all the non-Lewis acceptor moieties have exclusively different constitution. Even though L1 and its nature of coordination with Zn and Cd were same, their stabilization trends were drastically different; and this was clarified in this rigorous NBO analysis [28, 29].

3.2.6. Other Electronic Structure Properties. Other quantum chemical attributes such as ground state energy, dipole moment, polarizability, hyperpolarizability, $E_{\text{HOMO}-1}$, E_{HOMO} , E_{LUMO} , $E_{\text{LUMO}+1}$, and $\Delta E_{\text{L-H}}$, that is, energy gap between HOMO and LUMO, electronically calculated chemical potential (μ), chemical hardness (η), electron affinity (EA), ionization potential (IP), and global electrophilicity index (ω) are tabulated in Table 3 [30, 31]. These calculated quantum chemical descriptors could assist one to gain intuition on fundamental electronic structure properties of L1, ZnL1, and CdL1 systems. The theoretical basis for μ and η was initiated from hard soft acid base (HSAB) principle and based on first and second partial derivatives of stationary state molecular energy “ E ” against the number of electrons at constant marginal potential ν .

$$\mu = \left(\frac{\partial E}{\partial N} \right)_{\nu(r)}, \quad (7)$$

$$\eta = \frac{1}{2} \left(\frac{\partial^2 E}{\partial N^2} \right)_{\nu(r)}.$$

The ground state parabola model [b] of these equations can be given by

$$\mu = \frac{I + A}{2}, \quad (8)$$

$$\eta = \frac{I - A}{2},$$

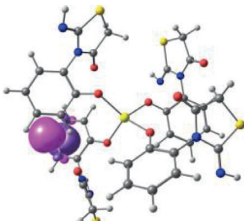
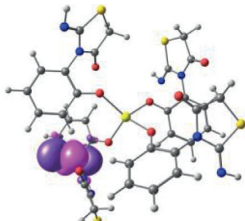
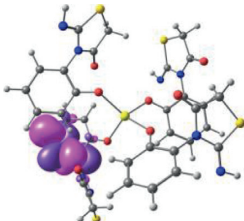
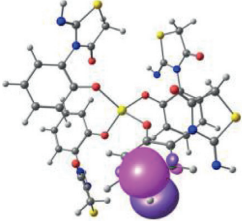
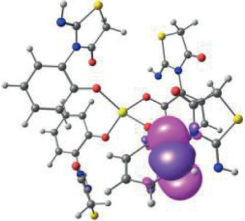
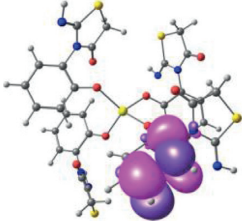
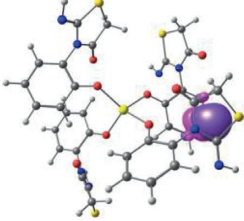
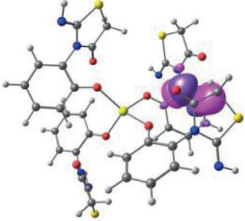
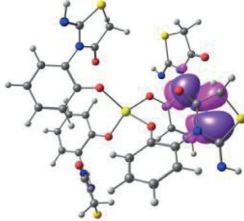
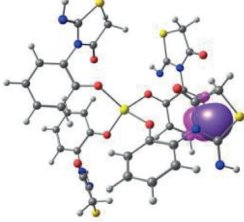
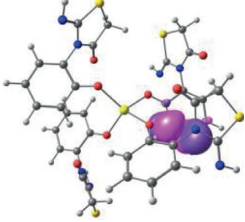
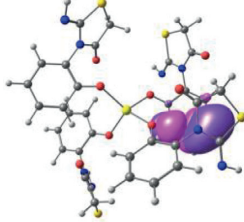
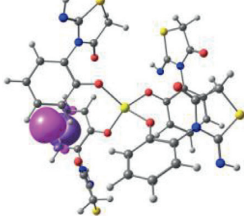
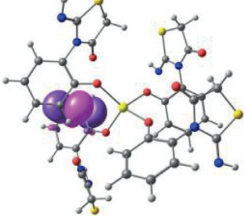
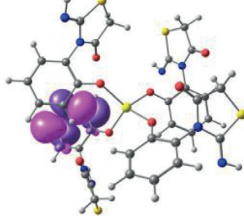
where I and A denote vertical ionization potential (IP) and electron affinity (EA), respectively. The global electrophilicity index (ω) [c] can be given by

$$\omega = \frac{\chi^2}{2\eta} = \frac{E_{\text{HOMO}}^2 + 2E_{\text{HOMO}}E_{\text{LUMO}} + E_{\text{LUMO}}^2}{4(E_{\text{LUMO}} - E_{\text{HOMO}})}, \quad (9)$$

where χ denotes Mulliken electronegativity and is correlated as $\mu = -\chi$.

The ground state energy reveals the ZnL1 and CdL1 their stability and complexation energies, respectively. In ZnL1 system, the complexation energy was found to be 4.51 a.u, and, in CdL1, the complexation energy was 4.49 a.u. Hence, the coordination of L1 with Zn has been more largely stabilized than the Cd metal. On considering FMOs, the pure L1 has large $\Delta E_{\text{L-H}}$ (5.06 eV) in comparison with ZnL1 (0.5023 eV) and CdL1 (0.4624 eV) which eventually results in absorption of visible light to give complimentary color. The dipole moment of L1 and ZnL1 has relatively same magnitude, whereas CdL1 has less dipole moment than the other two. The polarizability values are increasing pure L1 to ZnL1 and CdL1 complexes. The ZnL1 has more NLO property compared to CdL1 due to increased hyperpolarizability. The FMO related properties such as IP, A , η , ν , χ , μ , and ω have relative trend as shown in Table 3. Both metal complexes have lower hardness and higher softness,

TABLE 8: NBO profile of CdL1.

S. No	Donor	Acceptor	Stabilization
01	 <p>LP(1)C9/E_D (i): 0.9988e OE ($\epsilon_i^{(L)}$): -0.1181 a.u %E_D P: -/NLMOD: 0.00D</p>	 <p>π^* C4-C6/E_D (j): 0.3416e OE ($\epsilon_j^{(NL)}$): 0.0166 a.u %E_D P: 46.29$_{C4^-}$- 53.71$_{C6}$</p>	 <p>E(2) kJ mol$^{-1}$: 104.04 E(j)-E(i): 0.13 a.u F(i,j): 0.106 a.u</p>
02	 <p>LP(1)C37/E_D (i): 0.9780e OE ($\epsilon_i^{(L)}$): -0.1138 a.u %E_D P: -/NLMOD: 28.94D</p>	 <p>π^*C32-C34/E_D (j): 0.3103e OE ($\epsilon_j^{(NL)}$): 0.0332 a.u %E_D P: 47.06$_{C32^-}$- 52.94$_{C34}$</p>	 <p>E(2) kJ mol$^{-1}$: 96.58 E(j)-E(i): 0.15 a.u F(i,j): 0.106 a.u</p>
03	 <p>LP(1)C51/E_D (i): 0.9811e OE ($\epsilon_i^{(L)}$): -0.1159 a.u %E_D P: -/NLMOD: 26.71D</p>	 <p>π^*C46-C48/E_D (j): 0.3047e OE ($\epsilon_j^{(NL)}$): 0.0278 a.u %E_D P: 46.24$_{C46^-}$-53.76$_{C48}$</p>	 <p>E(2) kJ mol$^{-1}$: 95.58 E(j)-E(i): 0.14 a.u F(i,j): 0.105 a.u</p>
04	 <p>LP(1)C51/E_D (i): 0.9811e OE ($\epsilon_i^{(L)}$): -0.1159 a.u %E_D P: -/NLMOD: 26.71D</p>	 <p>π^*C47-C50/E_D (j): 0.2860e OE ($\epsilon_j^{(NL)}$): 0.0315 a.u %E_D P: 49.03$_{C47^-}$-50.97$_{C50}$</p>	 <p>E(2) kJ mol$^{-1}$: 91.93 E(j)-E(i): 0.15 a.u F(i,j): 0.104 a.u</p>
05	 <p>LP(1)C9/E_D (i): 0.9988e OE ($\epsilon_i^{(L)}$): -0.1181 a.u %E_D P: -/NLMOD: 0.00D</p>	 <p>π^*C5-C8/E_D (j): 0.2866e OE ($\epsilon_j^{(NL)}$): 0.0312 a.u %E_D P: 49.31$_{C5^-}$-50.69$_{C8}$</p>	 <p>E(2) kJ mol$^{-1}$: 91.76 E(j)-E(i): 0.15 a.u F(i,j): 0.105 a.u</p>

yet the reciprocal has been observed in L1. The negative magnitude of electronegativity could be chemical potential as mentioned above. The high " ω " value for metal complexes indicates a high molecular toxicity compared to pure organic system L1 [32–34].

4. Conclusion

In our earlier work, we reported the synthesis of L1 and its metal complexes with Zn and Cd metal. Spectroscopic and thermodynamic attributes were derived, and their structural features were confirmed earlier. The present work was extended to probe the biological sensitivity and theoretical investigations of both pure ligand and metal complexes. The biological evaluation of complexes against various pathogenic bacterial and fungal strains revealed that metal complexes had higher antimicrobial sensitivity than free ligand, but they were lower than standard drugs. However, the toxicity analysis has not been carried out and investigated. Theoretical and computational studies provide significant findings on structural features and electronic structure properties of target systems. The global minimum stationary point was derived from 3D PES scan surface analysis and further ground state properties were derived from that stationary point. The MEP and charge analysis on L1 and its metal complexes provides various point charge distributions and their reactive site profiles. Entire "O" atoms exhibit electrophilic nature and "N and S" atoms show nucleophilic nature on their potential surface. The highest molecular stabilization was satisfied by $LP \rightarrow \pi^*$ interaction in both pure L1 and its metal complexes. Additional electronic structure properties which are completely based on FMO gaps provide details on global harness, softness, ionization potential, electron affinity, and electrophilicity index. This thorough probe on the ground of biological and theoretical electronic structure provides deep understanding on 3-(2-hydroxyphenyl)-2-iminothiazolidin-4-one ligand and its Zn^{2+} and Cd^{2+} metal complexes.

Data Availability

No additional data have been used to support the conclusion.

Conflicts of Interest

The authors declare that they have no conflicts of interest.

Acknowledgments

The authors are grateful for the support provided by Department of Chemistry, CNCS, Haramaya University, Ethiopia.

Supplementary Materials

Supplementary Material S1: figures of optimized geometry and table of geometrical parameters of metal complexes ZnL1 and CdL1. Supplementary Material S2: table of various

atomic charges of metal complexes. (*Supplementary Materials*)

References

- [1] M. Wagner and C. Limberg, "Zinc complexes of a tripodal ligand containing three different N-heterocyclic donor functions," *Inorganica Chimica Acta*, vol. 362, no. 13, pp. 4809–4812, 2009.
- [2] M. El-Batouti, E. H. El-Mossalamy, and N. F. Al-Harby, "Electrical conductivity of charge transfer complexes of some thiophene schiff base complex with nitrobenzene acceptors," *Asian Journal of Chemistry*, vol. 27, no. 7, pp. 2719–2724, 2015.
- [3] G. G. Mohamed, M. M. Omar, and A. M. Hindy, "Metal complexes of Schiff bases: preparation, characterization, and biological activity," *Turkish Journal of Chemistry*, vol. 30, pp. 361–382, 2006.
- [4] H. Altintas, O. Ates, S. Birteksit, G. Otuk, M. Uzun, and M. Satana, "Synthesis of mannich bases of some 2,5-disubstituted-4-thiazolidinones and of their evaluation antimicrobial activities," *Turkish Journal of Chemistry*, vol. 29, pp. 425–435, 2005.
- [5] P. P. Deohate, J. P. Deohate, and B. N. Berad, "Synthesis of some Novel 1,2,4-dithiazolidines and their antibacterial and antifungal activity," *Asian Journal of Chemistry*, vol. 16, pp. 255–260, 2004.
- [6] J. G. Hyo, B. Kang, and R. Jeon, "Synthesis and biological activity of 5-(4-[2-(methyl-p-substituted phenylamino)ethoxy]benzyl)thiazolidine-2,4-diones," *Archives of Pharmacol Research*, vol. 30, pp. 1055–1061, 2007.
- [7] E. Ilhan and N. Ergent, "Synthesis and evaluation of substituted aryl thia-and oxazolidines for biological dyeing properties," *Archiv der Pharmazie*, vol. 325, p. 4625, 1992.
- [8] C. V. Kavitha, S. N. Basappa, S. N. Swamy et al., "Synthesis of new bioactive venlafaxine analogs: novel thiazolidin-4-ones as antimicrobials," *Bioorganic & Medicinal Chemistry*, vol. 14, no. 7, pp. 2290–2299, 2006.
- [9] Z. B. Gemechu, T. Kebede, E. G. Demissie, G. W. Woyessa, and S. B. Kassa, "Spectrophotometric study on the stability constants and thermodynamic parameters of Zn^{2+} , Cd^{2+} and Hg^{2+} complexes with Imino Thiazolidinone," *African Journal of Pure and Applied Chemistry*, vol. 9, no. 8, pp. 175–183, 2015.
- [10] P. S. Yadav, D. Prakash, and G. P. Senthilkumar, "Different methods of synthesis and diverse biological activities," *International Journal of Pharmaceutical Sciences and Drug Research*, vol. 3, pp. 1–7, 2011.
- [11] H. Ayalew, G. Reda, T. Gashaw, N. Babu, and R. Kumar Upadhyay, "Antimicrobial and dyeing properties of reactive dyes with thiazolidinon-4-one nucleus," *International Scholarly Research Notices*, vol. 8, Article ID 894250, 2014.
- [12] M. J. Frisch, G. W. Trucks, H. B. Schlegel et al., *Gaussian 09, Revision D.01*, Gaussian, Inc., Wallingford, CT, USA, 2013.
- [13] E. D. Glendenning, J. K. Badenhoop, A. E. Reed et al., "NBO 7.0," Theoretical Chemistry Institute, University of Wisconsin, Madison, WI, USA, 2018.
- [14] N. C. Desai, H. M. Satodiya, K. M. Rajpara, V. V. Joshi, K. Bhatt, and H. V. Vaghani, "Synthesis and evaluation of N-substituted thiazolidine-2,4-dione containing pyrazole as a potent antimicrobial agents," *Anti-Infective Agents*, vol. 12, no. 1, pp. 85–94, 2014.
- [15] M. S. Boobalan, D. Tamilvendan, S. Ramalingam, M. Amaladasan, G. Venkatesa Prabhu, and M. Bououdina, "Vibrational spectra and electronic structure of 3-((1H-pyrrol-1-yl) methyl) naphthalen-2-ol—a computational insight

- on antioxidant active Mannich base,” *Journal of Molecular Structure*, vol. 1081, pp. 159–174, 2015.
- [16] K. Anandhan, M. Susai Boobalan, P. Venkatesan, A. Ilangovan, M. P. Kaushik, and C. Arunagiri, “Crystallography and computational electronic structure investigations on 14-(3, 4, 5-trimethoxyphenyl)-14H-dibenzo[a,j]xanthene,” *Journal of Molecular Structure*, vol. 1097, pp. 185–198, 2015.
- [17] I. Mayer and P. Salvador, “Overlap populations, bond orders and valences for “fuzzy” atoms,” *Chemical Physics Letters*, vol. 383, no. 3-4, pp. 368–375, 2004.
- [18] M. Jeeva, G. V. Prabhu, M. S. Boobalan, and C. M. Rajesh, “Interactions and inhibition effect of urea-derived mannich bases on a mild steel surface in HCl,” *Journal of Physical Chemistry C*, vol. 119, no. 38, pp. 22025–22043, 2015.
- [19] D. Gajalakshmi, R. V. Solomon, V. Tamilmani, M. Boobalan, and P. Venuvanalingam, “A DFT/TDDFT mission to probe push-pull vinyl coupled thiophene oligomers for optoelectronic applications,” *RSC Advances*, vol. 5, no. 62, pp. 50353–50364, 2015.
- [20] J. P. Susairaj, S. Kaya, R. Ramamoorthy, E. Teju, and B. Maria Susai, “Spectra, electronic structure of 2-vinyl naphthalene and their oligomeric scaffold models: a quantum chemical investigation,” *Chemistry Africa*, vol. 3, no. 2, pp. 371–390, 2020.
- [21] K. Elangovan, M. S. Boobalan, A. Senthil, and G. Vinitha, “Investigation on growth, structural, characterization and DFT computing of imidazolium 3-nitrobenzoate (I3NB) single crystal-towards third order nonlinear optical applications,” *Journal of Molecular Structure*, vol. 1196, pp. 720–733, 2019.
- [22] I. G. Csizmadia, *Theory and Practice of MO Calculations on Organic Molecules*, Elsevier, Amsterdam, Netherlands, 1976.
- [23] P. J. Stephens, K. J. Jalkanen, and R. W. Kawiecki, “Theory of vibrational rotational strengths: comparison of a priori theory and approximate models,” *Journal of the American Chemical Society*, vol. 112, no. 18, pp. 6518–6529, 1990.
- [24] A. E. Reed, R. B. Weinstock, and F. Weinhold, “Natural population analysis,” *The Journal of Chemical Physics*, vol. 83, no. 2, pp. 735–746, 1985.
- [25] W. Frank and C. R. Landis, *Valency and Bonding: A Natural Bond Orbital Donor–Acceptor Perspective*, Cambridge University Press, Cambridge, UK, 2005.
- [26] W. Frank and C. R. Landis, “Natural Bond Orbitals and Extensions of Localized Bonding Concepts,” *Chemistry Education Research and Practice Journal*, vol. 2, pp. 91–104, 2001.
- [27] A. E. Reed and F. Weinhold, “Natural bond orbital analysis of near-Hartree-Fock water dimer,” *The Journal of Chemical Physics*, vol. 78, no. 6, pp. 4066–4073, 1983.
- [28] D. Gajalakshmi, M. S. Boobalan, R. Vijay Solomon, and V. Tamilmani, “Are vinyl coupled furan derivatives better than vinyl coupled thiophene derivatives for optoelectronic applications? Answers from DFT/TDDFT calculations,” *Computational Materials Science*, vol. 162, pp. 60–68, 2019.
- [29] M. S. Boobalan, S. Ramalingam, M. Amaladasan, D. Tamilvendan, G. Venkatesa Prabhu, and M. Bououdina, “A computational perspective on equilibrium geometry, vibrational spectra and electronic structure of antioxidant active Mannich base 1-[(Pyridin-2-yl amino) methyl] pyrrolidine-2,5-dione,” *Journal of Molecular Structure*, vol. 1072, pp. 153–172, 2014.
- [30] S. J. Pradeepa, M. S. Boobalan, D. Tamilvendan, N. Sundaraganesan, S. Sebastian, and K. Qian, “Spectra, electronic structure and molecular docking investigations on 3-(phenyl(p-tolylamino)methyl)naphthalen-2-ol—an experimental and computational approach,” *Journal of Molecular Structure*, vol. 1135, pp. 53–66, 2017.
- [31] M. Jeeva, M. S. Boobalan, and G. V. Prabhu, “Adsorption and anticorrosion behavior of 1-((pyridin-2-ylamino)(pyridin-4-yl)methyl)pyrrolidine-2,5-dione on mild steel surface in hydrochloric acid solution,” *Research on Chemical Intermediates*, vol. 44, no. 1, pp. 425–454, 2018.
- [32] R. G. Parr, L. V. Szentpály, and S. Liu, “Electrophilicity index,” *Journal of the American Chemical Society*, vol. 121, no. 9, pp. 1922–1924, 1999.
- [33] R. G. Parr, R. A. Donnelly, M. Levy, and W. E. Palke, “Electronegativity: the density functional viewpoint,” *The Journal of Chemical Physics*, vol. 68, no. 8, pp. 3801–3807, 1978.
- [34] R. G. Parr and W. Yang, *Density-Functional Theory of Atoms and Molecules*, Oxford University Press, New York, NY, USA, 1989.